# Field-theoretic model of inhomogeneous supramolecular polymer networks and gels

Aruna Mohan,[1] Richard Elliot,[2] and Glenn H. Fredrickson[1,2,3,a)]
[1]*Department of Chemical Engineering, University of California, Santa Barbara, California 93106, USA*
[2]*Materials Research Laboratory, University of California, Santa Barbara, California 93106, USA*
[3]*Department of Materials, University of California, Santa Barbara, California 93106, USA*

(Received 1 July 2010; accepted 14 September 2010; published online 1 November 2010)

We present a field-theoretic model of the gelation transition in inhomogeneous reversibly bonding systems and demonstrate that our model reproduces the classical Flory–Stockmayer theory of gelation in the homogeneous limit. As an illustration of our model in the context of inhomogeneous gelation, we analyze the mean-field behavior of an equilibrium system of reacting trifunctional units in a good solvent confined within a slit bounded by parallel, repulsive walls. Our results indicate higher conversions and, consequently, higher concentrations of gel following the gelation transition near the center of the slit relative to the edges. © *2010 American Institute of Physics*.
[doi:10.1063/1.3497038]

## I. INTRODUCTION

Owing to the recent emergence of novel materials such as self-healing rubbers,[1] stimuli-responsive polymers,[2] and self-assembled block copolymer architectures,[3] much interest has been generated in the design of supramolecular polymer networks for applications in nanotechnology, materials design, and biotechnology.[3–5] Monomeric units that associate via hydrogen bonding,[1,3,6,7] metal-ligand interactions,[2] ionic associations,[8] and hydrophobic interactions[9] have commonly been employed for the synthesis of thermoreversible supramolecular networks. In contrast to telechelic linear polymers, which retain only two terminal functional groups per chain, the functionality of a polymer network increases with the size of the network. Consequently, the presence of polyfunctional monomeric units, possessing three or more reactive functional groups that may covalently cross-link or form physical associations with other groups, enables the network to grow to macroscopic dimensions. The formation of an infinite network is referred to as gelation and marks a phase transition from a viscous liquid or a sol phase to an elastic gel phase.[10] Gelation is known to occur during the vulcanization of rubber, the molding of thermosetting resins, and the curing of coatings.[10] However, although branching presents the possibility of gelation, the design of tunable architectures for specific applications may be achieved by thermally controlling the degree of association and branching in thermoreversible networks.[6]

The theoretical study of network formation and gelation was pioneered by Flory,[10] who demonstrated the occurrence of infinite networks during polyfunctional condensation and identified the conditions for their formation. Flory's theory of gelation provides the weight fraction distribution and the number average and weight average degrees of polymerization in terms of a single parameter, namely, the fraction of reacted functional groups, denoted by $\alpha$. For a reactive system of end-functionalized $f$-arm units, the equilibrium weight average chain size is seen to diverge at a critical fractional conversion of $\alpha_c = 1/(f-1)$, signifying the gelation transition.[10] Subsequently, Stockmayer independently reproduced Flory's predictions.[11] The Flory–Stockmayer formalism is based largely on probabilistic and combinatorial arguments. Intramolecular reactions leading to the formation of rings are not accounted for in the pregelation regime. Flory and Stockmayer further considered the postgelation regime; however, their approaches differ in that the average size of the sol molecules beyond the gel point is fixed in Stockmayer's treatment, whereas it decreases as the conversion increases in Flory's approach.[11]

An alternative theoretical approach founded in statistical mechanics and graph theory was provided by Gordon and co-workers in a series of papers on chemical combinatorics and its application to gelation.[12–15] Gordon and co-workers related the reaction equilibria for the formation of all possible isomeric products from a system of polyfunctional units to the symmetries of the reactants and products. Furthermore, the symmetries were deduced via the enumeration of trees formed from the graphical representation of the polymer, whereby a correspondence was established between the weight fraction of $l$-mer in the equilibrium mixture and the number of distinct trees composed of $l$ nodes.[15,16] This approach was extended to treat the postgelation regime[17–19] within the framework of the theory of branching processes,[20] particularly in the form developed by Good,[21,22] yielding results in accord with those of Flory.[10] Gordon and co-workers further investigated copolymer networks and random cross-linked networks of vulcanized chains.[23,24]

Some recent studies on gelation include investigations of the phase behavior of associating polymer networks.[25–28] Methods similar to those originally developed by Polya[29] have been adopted in the enumeration of associating polymers,[30] and Refs. 31 and 32 treat the conformational

a)Author to whom correspondence should be addressed. Electronic mail: ghf@mrl.ucsb.edu.

 

statistics of branched polymers. However, these studies do not take into consideration the effect of polymer symmetry on the equilibrium distribution. A recent review of developments in the theory of polycondensation is provided in Ref. 33. The structural and elastic properties of polymer networks have been previously investigated by utilizing the replica method for averaging over all possible realizations of randomly cross-linked network structures.[34] Edwards and co-workers[35,36] investigated the elasticity of gels and networks, and the origin of network rigidity is rationalized in Ref. 37 within the framework of replica theory. In the present study, however, we are interested in investigating the equilibrium properties of networks resulting from the self-assembly of telechelic branched chain units.

Inhomogeneous networks and gels arise in many practical situations, such as the formation of ordered microstructures during the copolymerization of distinct branched chain units (for example, interpenetrating networks) and the syneresis phenomena in gels encountered with rapid changes in solvent quality. The description of inhomogeneous polymer networks entails full consideration of the spatially dependent conformational entropies of all isomeric chain configurations, with the equilibrium distribution of chains being dictated by their topologies. At present, such a description is lacking, and it is the goal of our study to present a field-theoretic model of inhomogeneous networks. We consider the polymerization of $f$-arm units and employ the method of Gordon and co-workers to quantify the resulting reaction equilibria. The aforementioned method is embedded within a field-theoretic model, in which full account is taken of the configurational entropies of all chains. As a first application of our new formalism to inhomogeneous gelation, we consider gelation in a good solvent under one-dimensional confinement for the case $f=3$. The present work serves as a framework that may be generalized to treat random and copolymer networks. This paper is organized as follows. Our theoretical formulation is presented in Sec. II. We present our results in Sec. III, and Sec. IV contains a summary of our findings and discusses possible extensions of our work. The details of our calculations, as well as some limiting cases[38,39] of our formalism, are contained in the Appendix and in the supplementary material.[40]

## II. FIELD-THEORETIC MODEL

Here, we consider the equilibrium behavior of a system of $f$-arm units, whose arms are functionalized with end groups that react with each other to form polymer networks. We denote by $N$ the degree of polymerization of each arm of the $f$-arm structure. The ideal chain statistics are described by the continuous Gaussian chain model. Further, we assume that the polymers are dissolved in a good solvent and treat the solvent implicitly via the introduction of pairwise excluded volume interactions among the chain segments. The treatment of more general models, such as explicit solvent conditions, constitutes a straightforward extension of the current treatment.[41] The equilibrium behavior of the above reacting system is amenable to field-theoretic treatment in the grand canonical ensemble. In this section, we outline the salient features of our field-theoretic model, while the details are relegated to the Appendix.

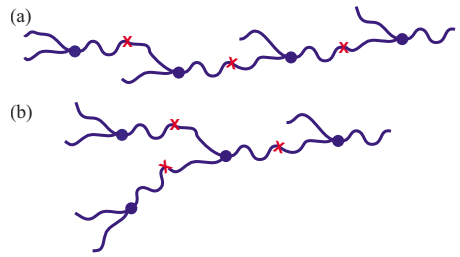


FIG. 1. Schematic illustration of the linear (a) and branched (b) isomeric forms of a polymer composed of four monomeric units with $f=3$. The circles represent nodes and the crosses represent reacted terminals.

The partition function in the grand canonical ensemble is given by the expression[41]

$$\mathcal{Z}_G = \int \mathcal{D}w e^{-H_G[w]}, \tag{1}$$

with the effective Hamiltonian

$$H_G[w] = \frac{1}{2u_0}\int d^3\mathbf{r}w^2(\mathbf{r}) - \sum_{l=1}^{\infty}\sum_{k} z_{l,k}VQ_{l,k}[iw] \tag{2}$$

in units of the thermal energy scale $k_BT$, where $k_B$ denotes Boltzmann's constant, $T$ denotes the temperature, and $V$ is the volume of the system. Equation (1) involves a path integral over all possible field configurations $w(\mathbf{r})$. The terms on the right hand side of Eq. (2) arise, respectively, from the repulsive interactions among polymer segments mediated by the field $w(\mathbf{r})$ and the configurational entropy of a chain in the field $iw(\mathbf{r})$, summed over all chain sizes $l$ and over all isomeric configurations, indexed by $k$, for each $l$. The parameter $u_0(>0)$ represents the strength of excluded volume interactions, and $z_{l,k}$ and $Q_{l,k}[iw]$ denote, respectively, the activity and the single-chain partition function in the field $iw(\mathbf{r})$ of the $l$-mer in its $k$th isomeric form. As an illustration of the various isomers obtained for a given chain length, Fig. 1 depicts the isomeric structures representing chains composed of four monomers with $f=3$.

The activity $z_{l,k}$ is related to the activity of a single monomeric unit, denoted by $z$, through the law of mass action

$$\frac{z_{l,k}}{z^l} = \frac{1}{\rho_{\text{ref}}^{l-1}}e^{-\Delta G_{l,k}/k_BT}, \tag{3}$$

where $\rho_{\text{ref}}$ denotes an arbitrarily chosen reference density and $\Delta G_{l,k}$ denotes the free energy of formation of the $l$-mer in its $k$th isomeric form from its $f$-arm monomeric constituents.[42,43] The right hand side of Eq. (3) represents the equilibrium constant $K_{\text{eq }l,k}$ for the formation of the $k$th isomer of $l$ units.

The equilibrium constant is conventionally computed in statistical thermodynamics from the ratio of the partition functions of products and reactants, where the partition functions contain contributions from translational and internal degrees of freedom. The contribution to the partition function from internal degrees of freedom is generally decomposed

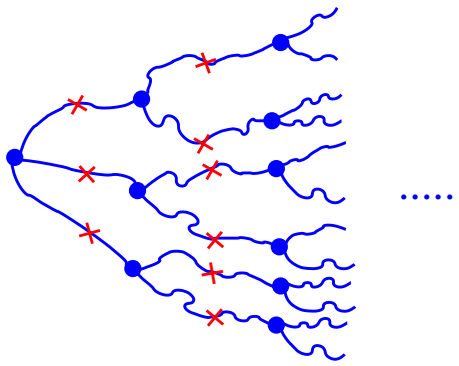

FIG. 2. Schematic illustration of a treelike polymer structure for $f=3$. The circles represent nodes and the crosses represent reacted terminals.

further into contributions from rotational, vibrational, electronic, and nuclear modes.[42,43] The dependence of the equilibrium constants for the formation of various isomeric products on their respective structures was quantified by Gordon and co-workers,[42] who made the observation that the rotational partition function is inversely proportional to the rotational symmetry number, which, in turn, is determined by the chemical structure. In particular, with the neglect of intramolecular reactions, the polymers may be represented as treelike structures, as illustrated by Fig. 2 for $f=3$. Gordon and co-workers[12,15] exploited these observations in establishing the relation between the symmetry of a polymer and its free energy of formation.

The free energy of formation of the $k$th isomer of $l$ units now takes the form[12]

$$\Delta G_{l,k} = (l-1)\Delta G^0 - T\Delta S_{\text{comb } l,k}, \tag{4}$$

where $\Delta G^0$ represents a "fundamental" free energy of the bond formation, assumed to be independent of polymer size and structure. The term $\Delta S_{\text{comb } l,k}$ denotes the combinatorial entropy deriving from the inverse dependence of the rotational partition function on the symmetry number and is given by the expression

$$\Delta S_{\text{comb } l,k} = k_{\text{B}} \ln\left(\frac{|G_{\text{M}}|^l}{|G_{l,k}|}\right). \tag{5}$$

In the above, $|G_{\text{M}}|$ and $|G_{l,k}|$ denote the symmetry numbers of a single $f$-arm unit and the $l$-mer in its $k$th isomeric form, respectively. The symmetry number of a polymer was discovered to be inversely related to the number of distinct rooted, ordered trees[44,45] that may be obtained from the graph of the polymer.[12,15] Upon employing the combinatorial entropy computed by Gordon and co-workers, Eq. (3) reduces to the following:

$$z_{l,k} = z\frac{T_{l,k}}{l}\left(\frac{zf}{\rho_{\text{ref}}}e^{-\Delta G^0/k_{\text{B}}T}\right)^{l-1}. \tag{6}$$

In the above, $T_{l,k}$ denotes the number of distinct rooted, ordered trees yielded by the graph of the $l$-mer in its $k$th isomeric form, and the factor $1/l$ arises from symmetry considerations. The interested reader may consult the Appendix and Refs. 12–15 for details.

Equation (2), taken in conjunction with Eq. (6), yields a complete field-theoretic model of our system. However, it remains to perform the summations over chain sizes $l$ and isomer conformations $k$. This is achieved by means of generating functions analogous to those widely employed in discrete mathematics.[15,46,47] We present only our final results here, and the reader is referred to the Appendix for the mathematical details. The Hamiltonian adopts the final form

$$H_{\text{G}}[w] = \frac{1}{2u_0}\int d^3\mathbf{r}w^2(\mathbf{r}) - z\int_0^1 d\theta\int d^3\mathbf{r}F_0(\mathbf{r},\theta,[iw]). \tag{7}$$

In Eq. (7), a generating function $F_0$ in the auxiliary variable $\theta$ has been introduced, defined recursively by the following equations:

$$F_0(\mathbf{r},\theta,[iw]) = \left[q_0(\mathbf{r},N,[iw]) + \lambda\theta\int d^3\mathbf{r}'G(\mathbf{r},\mathbf{r}',2N)F_1(\mathbf{r}',\theta,[iw])\right]^f,$$

$$F_1(\mathbf{r},\theta,[iw]) = \left[q_0(\mathbf{r},N,[iw]) + \lambda\theta\int d^3\mathbf{r}'G(\mathbf{r},\mathbf{r}',2N)F_1(\mathbf{r}',\theta,[iw])\right]^{f-1}, \tag{8}$$

where we have introduced the notation

$$\lambda = \frac{zf}{\rho_{\text{ref}}}e^{-\Delta G^0/k_{\text{B}}T}. \tag{9}$$

The term $q_0(\mathbf{r},s,[iw])$ appearing above is a "free chain" propagator, yielding the statistical weight for the segment at contour location $s$ to lie at spatial position $\mathbf{r}$ for a chain starting from a free end. The term $G(\mathbf{r},\mathbf{r}',s)$ represents the Green's function for diffusion (chain propagation) in the field $iw(\mathbf{r})$ and is related to $q_0$ via the expression

$$q_0(\mathbf{r},s,[iw]) = \int d^3\mathbf{r}'G(\mathbf{r},\mathbf{r}',s). \tag{10}$$

The second term within the parentheses on the right hand side of Eq. (8) represents the statistical weight for the segment to lie at spatial position $\mathbf{r}$ starting from a point at a contour distance of $2N$ along the polymer, where the latter point is characterized by the statistical weight $F_1(\mathbf{r}',\theta,[iw])$. In the context of the tree structure illustrated in Fig. 2, the first term within the parentheses on the right hand side of Eq. (8) propagates the tree conformation from a free or unreacted arm end to the center point of the same unit by a contour distance of $N$, while the second term propagates from the center point of a unit to that of the preceding unit by a contour distance of $2N$, with the factor $\lambda$ signifying a bond between the two units. Note that $f$ arms emanate from the root unit, whereas $f-1$ arms emanate from each succeeding unit. Consequently, the powers of $f$ and $f-1$ appearing in Eq. (8) represent all arms emanating from the root unit and the remaining units, respectively, whereby $F_0$ serves as the generating function for the root unit and $F_1$ for all other units.

(The term "node" is henceforth employed to denote the center point of an $f$-arm unit, while "terminal" refers to the end point of an arm.)

It is now evident that the recursive structure of Eq. (8) reproduces all possible tree conformations that arise from the infinite tree structure illustrated in Fig. 2, with the coefficient of $\theta^{l-1}$ in $F_0$ representing the statistical weight, summed over all rooted, ordered trees of $l-1$ chemical bonds or $l$ nodes, for the root node to lie at $\mathbf{r}$. The generating functions $F_0$ and $F_1$ are reminiscent of chain propagators[41] conventionally employed in polymer field theory; however, they additionally incorporate a sum over rooted, ordered trees weighted by powers of the auxiliary variable $\theta$. Consequently, the use of the above generating functions facilitates computation of the summations over $l$ and $k$ in Eq. (2), appropriately weighted by the corresponding activities $z_{l,k}$ [cf. Eq. (6)], yielding the final form of Eq. (7). Finally, we remark that the integral over the auxiliary variable $\theta$ in Eq. (7) arises from the presence of the factor $1/l$ in Eq. (6).

In the grand canonical ensemble, the segment density takes the standard form[41]

$$\rho(\mathbf{r}) = -\sum_{l,k} z_{l,k} V \frac{\delta Q_{l,k}[iw]}{\delta iw(\mathbf{r})}. \tag{11}$$

As elaborated in the Appendix, Eq. (11) may be expressed in terms of the generating function $F_1$, yielding the following simplified expression for the segment density:

$$\rho(\mathbf{r}) = zf \int_0^N ds \left\{ \left[ q_0(\mathbf{r},s,[iw]) + \lambda\theta \times \int d^3\mathbf{r}_1 G(\mathbf{r},\mathbf{r}_1,N+s) F_1(\mathbf{r}_1,\theta,[iw]) \right] \times \int d^3\mathbf{r}_2 G(\mathbf{r},\mathbf{r}_2,N-s) F_1(\mathbf{r}_2,\theta,[iw]) \right\}_{\theta=1}. \tag{12}$$

The reader is referred to the Appendix for an interpretation of the terms appearing in Eq. (12). Furthermore, the densities of reacted and unreacted end segments may be evaluated, enabling the computation of the local fractional density of reacted ends, denoted by $\alpha(\mathbf{r})$, which serves as a generalization of Flory's $\alpha$ parameter, representing fractional conversion. The density of unreacted $f$-arm units, and the number average and weight average degrees of polymerization, denoted by $N_n$ and $N_w$, respectively, are also readily computed. The above formulation is applicable in both the pre- and the postgelation regimes with the appropriate selection of the roots of $F_1$ from Eq. (8). The details are contained in the Appendix.

While the above formulation is valid generally, the results presented in this study will be restricted to the mean-field approximation. For convenience, we introduce the following scaled variables:

$$\bar{w} = iNw, \quad \bar{z}_{l,k} = \frac{z_{l,k}}{\rho_0/N},$$

$$\bar{\mathbf{r}} = \frac{\mathbf{r}}{R}, \quad \bar{V} = \frac{V}{R^3}, \tag{13}$$

$$\phi = \frac{\rho}{\rho_0},$$

where we employ a reference unit of length $R$, which is the radius of gyration of one arm of the $f$-arm unit, related to the Kuhn step length $b$ by the expression $R^2 = Nb^2/6$. The density $\rho_0$ introduced above is the average total segment density, defined as $\rho_0 = \int d^3\mathbf{r}\rho(\mathbf{r})/V$.

The self-consistent field equations arise from the saddle point condition, $\delta H_G[w]/\delta w(\mathbf{r}) = 0$,[41] yielding, in scaled form,

$$\bar{w}(\bar{\mathbf{r}}) = (u_0\rho_0 N)\phi(\bar{\mathbf{r}}). \tag{14}$$

In addition, the reduced density $\phi(\bar{\mathbf{r}})$ [cf. Eq. (A14)] satisfies the following normalization condition by definition:

$$\frac{1}{\bar{V}} \int_{\bar{V}} d^3\bar{\mathbf{r}}\phi(\bar{\mathbf{r}}) = 1. \tag{15}$$

The scaled activity $\bar{z} = z/(\rho_0/N)$, which determines the polymer activities via Eq. (6), is in turn treated as a variable to be chosen such that the normalization condition of Eq. (15) is satisfied. The elimination of $\bar{z}$ enables us to minimize the number of parameters required to characterize our system. Equation (8) may be recast in terms of the above scaled variables by rewriting Eq. (9) in the equivalent form

$$\lambda = \frac{\bar{z}f}{N} e^h, \tag{16}$$

with

$$h = \frac{-\Delta G^0}{k_B T} + \ln\left(\frac{\rho_0}{\rho_{ref}}\right). \tag{17}$$

Equations (8) and (14)–(16) reveal that the behavior of the system for a given $f$ is determined by three parameters: an excluded volume parameter $u_0\rho_0 N$, a parameter controlling the reaction strength, $e^h/N$, and the scaled system volume $\bar{V}$. The field $\bar{w}$, reduced density $\phi$, and activity $\bar{z}$ are determined such that Eqs. (14) and (15) are satisfied. Our results for homogeneous gelation for several values of $f$ and for gelation under one-dimensional confinement in a slit of dimensionless width $\bar{L} = 10$ for the case $f = 3$ are presented in Sec. III. The value $N = 100$ is employed throughout this study.

## III. RESULTS

We first consider gelation in a homogeneous system for several values of $f$. The homogeneous solution may be obtained analytically or numerically by adopting the methods presented in the supplementary material.[40]

Figure 3 depicts the number average and weight average degrees of polymerization, $N_n$ and $N_w$, as functions of the fractional conversion $\alpha$ for values of $f$ ranging from 3 to 7.

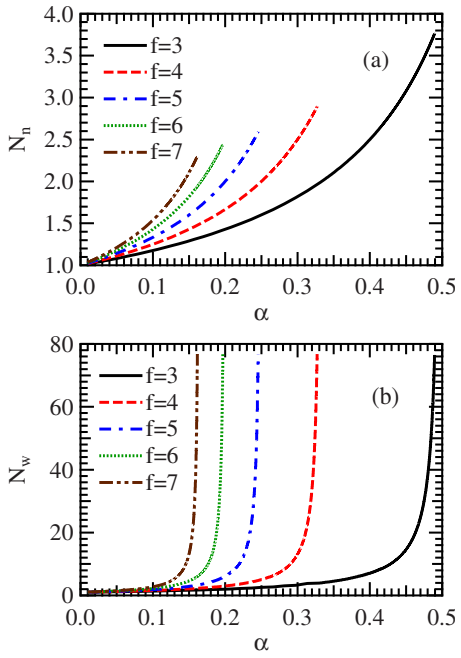


FIG. 3. (a) $N_n$ (number average degree of polymerization) vs $\alpha$ (fractional conversion) and (b) $N_w$ (weight average degree of polymerization) vs $\alpha$ for several values of $f$ with $u_0\rho_0 N=1$ in a homogeneous system.

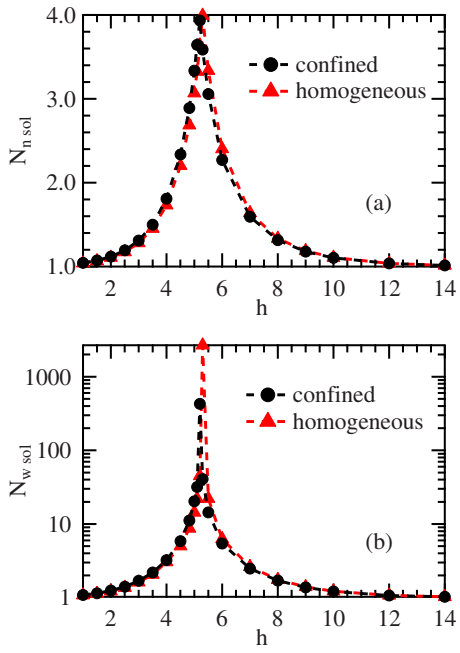


FIG. 5. (a) $N_{n\ sol}$ (number average degree of polymerization in the sol phase) vs $h$ and (b) $N_{w\ sol}$ (weight average degree of polymerization in the sol phase) vs $h$ under confinement with $u_0\rho_0 N=1$ and $\bar{L}=10$ (circles) and in a homogeneous system (triangles) for $f=3$. The dashed lines are meant to guide the eye.

In accord with Flory's predictions, $N_w$ diverges at the critical value $\alpha_c=1/(f-1)$. The corresponding value of $N_n$ is in agreement with Flory's prediction, $N_n=(f-1)/(f/2-1)$.[10] These results are unchanged upon varying the excluded volume parameter $u_0\rho_0 N$. Figure 4 illustrates the dependence of $\alpha$, the fractional conversion in the sol phase, $\alpha_{sol}$, and the reduced densities of sol and unreacted $f$-arm units, $\phi_{sol}$ and $\phi_{mon}$, respectively, on the parameter $h$ characterizing the strength of reactions for the case $f=3$. Explicit expressions for these quantities may be found in the supplementary material.[40] Prior to the gel point, $\alpha_{sol}=\alpha$ and $\phi_{sol}=1$. However, $\alpha_{sol}$ and $\phi_{sol}$ decrease continuously to 0 after the gel point is crossed, as expected, while $\alpha$ increases to unity. These results are consistent with prior studies on homogeneous gelation.[10,17,19]

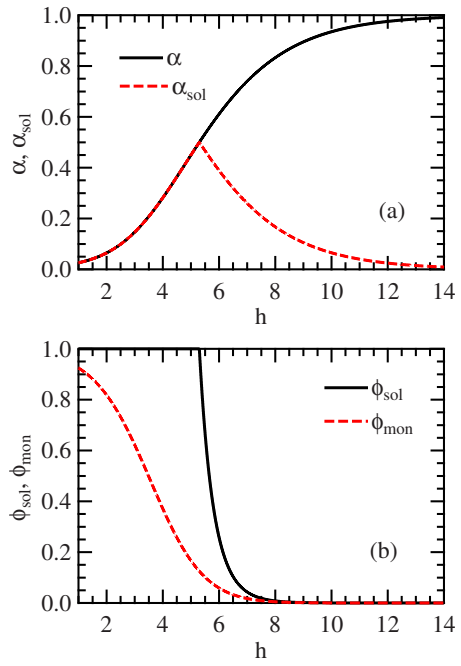


FIG. 4. (a) $\alpha$ (fractional conversion) vs $h$ (solid line) and $\alpha_{sol}$ (fractional conversion in the sol phase) vs $h$ (dashed line), and (b) $\phi_{sol}$ (reduced density in the sol phase) vs $h$ (solid line) and $\phi_{mon}$ (reduced density of unreacted monomeric units) vs $h$ (dashed line) in a homogeneous system with $f=3$.

We next consider the equilibrium behavior of a reacting system of three-arm units confined between two parallel, repulsive walls separated by a nondimensional distance of $\bar{L}$ measured in units of $R$. We denote by $x$ the nondimensional distance $\bar{\mathbf{r}}\cdot\hat{\mathbf{x}}$ measured across the slit, where $\hat{\mathbf{x}}$ is the unit vector transverse to the walls, with the wall coordinates given by $x=0$ and $x=\bar{L}$. We select $f=3$ and $\bar{L}=10$ for the sake of illustration, although our method is generally applicable to situations involving inhomogeneous gelation. The details of our numerical procedure[48,49] for the confined system are presented in the supplementary material.[40]

Figure 5 provides a comparison between the number average and weight average degrees of polymerization in the sol phase, $N_{n\ sol}$ and $N_{w\ sol}$, as functions of $h$ in the confined system and those in the homogeneous system. The excluded volume parameter $u_0\rho_0 N$ is set to 1 in the confined system. Prior to the gel point, $N_{n\ sol}\equiv N_n$ and $N_{w\ sol}\equiv N_w$. Beyond the gel point, $N_{n\ sol}$ and $N_{w\ sol}$ decrease to 0 as $h$ increases. This behavior is consistent with the expectation that the macroscopic network in the gel phase reacts with the smaller molecules in the sol phase as the total fractional conversion $\alpha$ increases to 1 after the gel point is crossed. Figure 5 reveals that the gel point, corresponding to the divergence in $N_w$, occurs at a slightly lower value of $h$ between 5.1 and 5.2 in the confined system relative to the homogeneous system,

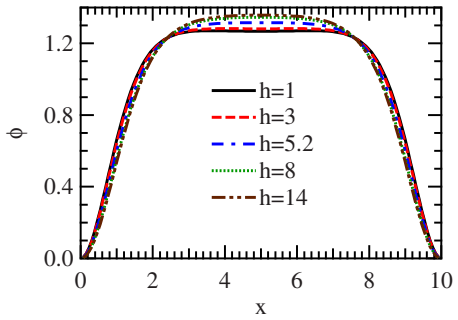


FIG. 6. $\phi(x)$ (reduced density) vs $x$ for $h=1$ (solid line), 3 (dashed line), 5.2 (dashed-dotted line), 8 (dotted line), and 14 (dashed-double-dotted line) under confinement, with $f=3$, $u_0\rho_0N=1$, and $\bar{L}=10$.

where $h=5.3$ at the gel point. This observation may be explained by the fact that the density in the confined system is higher than its average value near the center of the slit (Fig. 6), thereby enhancing the bonding reactions near the slit center.

The density profiles in the confined system are illustrated in Fig. 6, which depicts the reduced density $\phi(x)$ versus $x$ for several values of $h$, with $u_0\rho_0N=1$. As expected, $\phi(x)$ vanishes at the walls and rises to its maximum value near the center of the slit. The density profiles are found to exhibit only a weak dependence on $h$. The length scale over which $\phi(x)$ increases from zero at the walls to a plateau near the center of the slit corresponds to the correlation length in bulk.[41] As expected, this length scale shows an increase, although slight, as $h$ is increased. The correlation length is determined primarily by the value of $u_0\rho_0N$, as discussed later in this section.

Figure 7 depicts the local fractional conversion $\alpha(x)$ and the local density of unreacted three-arm units as a fraction of the total local density, $\phi_{\text{mon}}(x)/\phi(x)$, as functions of $x$ for

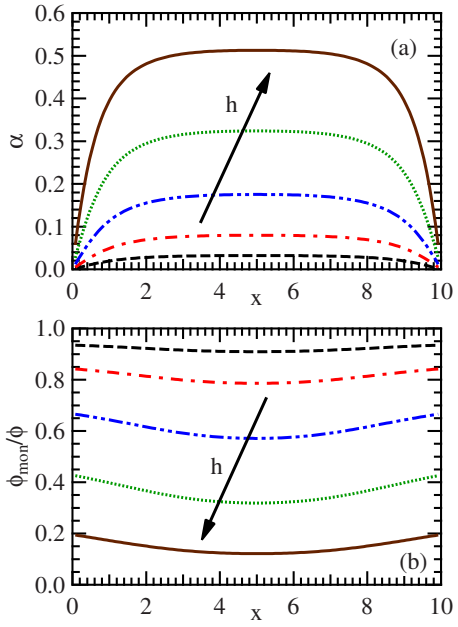


FIG. 7. (a) $\alpha(x)$ vs $x$ and (b) $\phi_{\text{mon}}(x)/\phi(x)$ vs $x$ in the pregelation regime for $h=1$ (dashed line), 2 (dashed-dotted line), 3 (dashed-double-dotted line), 4 (dotted line), and 5.1 (solid line) under confinement, with $f=3$, $u_0\rho_0N=1$, and $\bar{L}=10$. The arrow indicates the direction of increasing $h$.

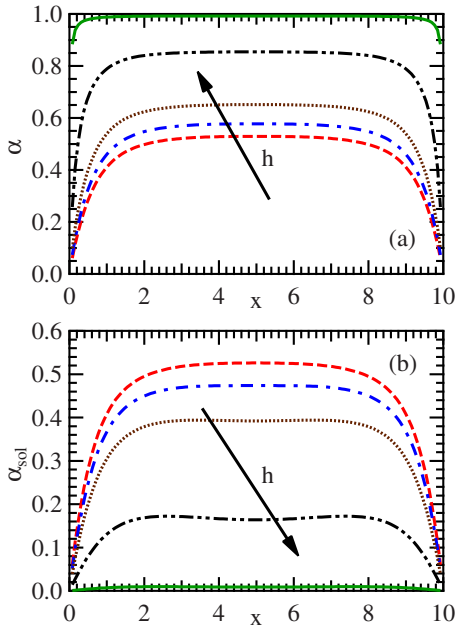


FIG. 8. (a) $\alpha(x)$ vs $x$ and (b) $\alpha_{\text{sol}}(x)$ vs $x$ in the postgelation regime for $h=5.2$ (dashed line), 5.5 (dashed-dotted line), 6 (dotted line), 8 (dashed-double-dotted line), and 14 (solid line) under confinement, with $f=3$, $u_0\rho_0N=1$, and $\bar{L}=10$. The arrow indicates the direction of increasing $h$.

several values of $h$ prior to the gel point, with $u_0\rho_0N=1$. Higher values of $\alpha(x)$ and, concomitantly, lower values of $\phi_{\text{mon}}(x)/\phi(x)$ are found to occur at the center of the slit, corresponding to higher densities at the center. The corresponding homogeneous values of $\alpha$ are smaller than the maximum values of $\alpha(x)$ in the confined system, while the homogeneous values of $\phi_{\text{mon}}$ exceed the corresponding values of $\phi_{\text{mon}}(x)/\phi(x)$ at the center of the confined system.

Fractional conversions and densities beyond the gel point for several values of $h$ with $u_0\rho_0N=1$ are illustrated in Figs. 8 and 9. It is evident from Fig. 8 that the total fractional conversion $\alpha(x)$ increases to approach a uniform value of 1 as $h$ is increased beyond the gel point. However, the fractional conversion in the sol phase, $\alpha_{\text{sol}}(x)$, decreases to 0 upon increasing $h$ beyond the gel point as molecules in the sol phase react with the gel. A slight dip in $\alpha_{\text{sol}}(x)$ is observed at the center of the slit, possibly owing to the occurrence of a larger fraction of gel at the center. Figure 9 reveals that the segment densities of sol and unreacted three-arm units as a fraction of the local segment density, $\phi_{\text{sol}}(x)/\phi(x)$ and $\phi_{\text{mon}}(x)/\phi(x)$, respectively, exhibit a minimum at the center of the slit, indicating the presence of a higher concentration of gel at the center. The densities of sol and unreacted units decrease to 0 with an increase in $h$ as $\alpha$ approaches 1.

The effect of varying $u_0\rho_0N$ is illustrated in Fig. 10, which depicts the reduced density $\phi(x)$, fractional conversion $\alpha(x)$, and fractional segment density $\phi_{\text{mon}}(x)/\phi(x)$ as a function of $x$ for several values of $u_0\rho_0N$, with $h=5$. Similar results not presented here are obtained at other values of $h$. Lower values of $u_0\rho_0N$ indicate weaker repulsive interactions among polymer segments. As a result, higher values of $\phi(x)$ and $\alpha(x)$ and, concomitantly, lower values of $\phi_{\text{mon}}(x)/\phi(x)$ are observed near the center of the slit for lower values of $u_0\rho_0N$. The healing of the density profile from zero at the

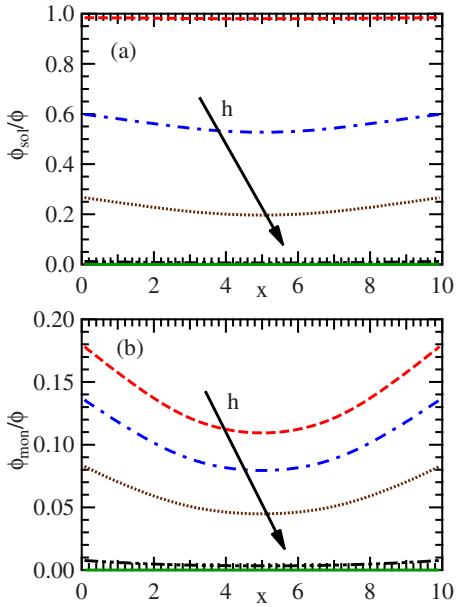


FIG. 9. (a) $\phi_{sol}(x)/\phi(x)$ vs $x$ and (b) $\phi_{mon}(x)/\phi(x)$ vs $x$ in the postgelation regime for $h=5.2$ (dashed line), 5.5 (dashed-dotted line), 6 (dotted line), 8 (dashed-double-dotted line), and 14 (solid line) under confinement, with $f=3$, $u_0\rho_0N=1$, and $\bar{L}=10$. The arrow indicates the direction of increasing $h$.

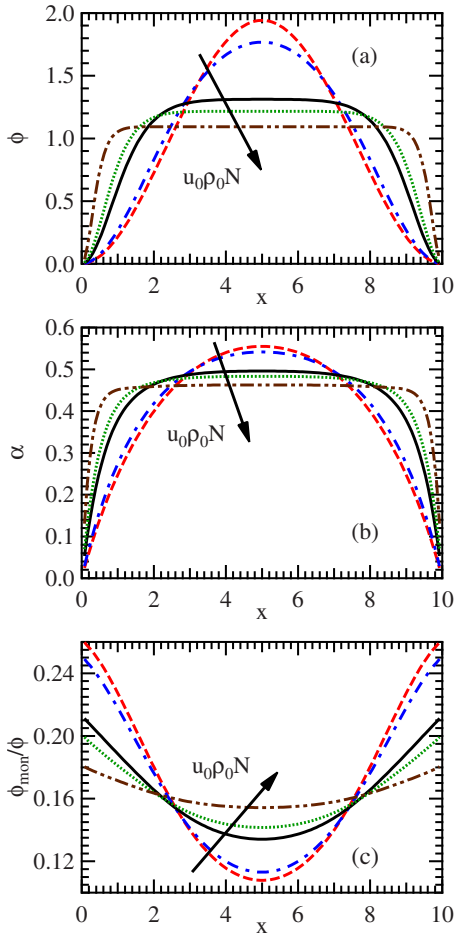


FIG. 10. (a) $\phi(x)$ vs $x$, (b) $\alpha(x)$ vs $x$, and (c) $\phi_{mon}(x)/\phi(x)$ vs $x$ under confinement, with $f=3$, $\bar{L}=10$, $h=5$, and $u_0\rho_0N=0.01$ (dashed line), 0.1 (dashed-dotted line), 1 (solid line), 2 (dotted line), and 10 (dashed-double-dotted line). The arrow indicates the direction of increasing $u_0\rho_0N$.

walls to the maximum value at the center of the slit occurs over a length scale corresponding to the correlation length in bulk.[41] The structure factor and the correlation length for the reacting $f$-arm system are derived by a weak inhomogeneity expansion (random phase approximation) in the supplementary material.[40] As observed earlier, the correlation length exhibits only a weak dependence on $h$, and it is shown in the supplementary material[40] that the correlation length possesses the scaling behavior $\xi_E \sim R/\sqrt{2u_0\rho_0N}$ for a concentrated system, similar to the behavior of nonreactive linear chains in bulk. This relation was confirmed to be consistent with the data in Fig. 10 for $u_0\rho_0N \gtrsim 1$.

While the results presented so far correspond to a confinement width of $\bar{L}=10$, other values of $\bar{L}$ ranging from 10 to 80 exhibit similar behavior, with the screening length scales remaining unaffected by the value of $\bar{L}$. No sol-gel phase separation was observed to take place in our studies, consistent with the expectation that phase separation does not occur in a good solvent, as noted in prior studies.[25]

## IV. DISCUSSION

In this study, we present a field-theoretic model of an inhomogeneous reacting system of end-functionalized $f$-arm units at equilibrium. Our model adopts the method of Gordon and co-workers[12–15] for quantifying the equilibrium constants for the formation of various isomeric products in terms of the symmetries of reactants and products, where the latter is related to the simpler problem of tree enumeration. The aforementioned quantification of reaction equilibria is embedded within a field-theoretic framework with full account of all isomeric chain conformations. Our model is applicable to both the pregelation and the postgelation regimes.

It is demonstrated that our model reproduces the classical theory of gelation developed independently by Flory,[10] Stockmayer,[11] and Gordon and co-workers[12–15] in the homogeneous limit. Furthermore, the present model is generally applicable to situations involving inhomogeneous gelation and can be applied with or without a simplifying mean-field approximation. As an illustration, we presented here a numerical investigation of gelation under one-dimensional confinement for the case $f=3$ and invoking the mean-field approximation.

Inherent in the tree approximation used in our formalism is the assumption that intramolecular reactions leading to ring formation are negligible. This assumption is also fundamental to the theory of branching processes.[20] Therefore, we do not account for rings in our field-theoretic description of polymer configurations. While the neglect of intramolecular reactions may lead to quantitative errors in the results, particularly after the gel point is crossed, it is nevertheless expected that the results we observe are qualitatively valid and are expected to shed new insights into network-forming inhomogeneous polymer systems.

The present investigation constitutes a new framework for the treatment of inhomogeneous gelation in more general situations. For example, copolymer networks comprising two or more distinct polymers may exhibit a range of ordered microstructures determined by the interplay between en-

tropic and enthalpic contributions to the free energy. Field-theoretic models of network behavior are expected to facilitate the prediction of the resulting network morphologies, their gelation behavior, and their quasistatic linear and nonlinear elastic properties. The formulation and analysis of such models will be the subject of future work.

## ACKNOWLEDGMENTS

This work was partially supported by the National Science Foundation through Award No. NSF-DMR09-04499. The project also received partial support from the NSF MRSEC Program under Award No. DMR05-20415 and made use of the MRL Central Facilities at UCSB, a member of the NSF-funded Materials Research Facilities Network (www.mrfn.org).

## APPENDIX: THEORETICAL FORMULATION

### 1. Field theory in the grand canonical ensemble

Consider a system of reactive $f$-arm units at equilibrium, with the equilibrium mixture containing $\{n_{l,k}\}$ chains of $l$ units in their $k$th isomeric form. The canonical partition function is given by the expression

$$\mathcal{Z}_C = \frac{1}{\Pi_{l,k} n_{l,k}! \lambda^{3fNn_0}} \int \prod_{l,k} \mathcal{D}R_{l,k} e^{-\beta(U_0+U_1)}, \tag{A1}$$

where $n_0=\Sigma_{l,k} l n_{l,k}$ is the initial number of $f$-arm units, $\beta=(k_B T)^{-1}$, and the notation $\int \mathcal{D}R_{l,k}$ implies a functional integral over all space curves $R_{l,k}$ describing the polymer configurations. The potential $U_0$ denotes the potential energy of the continuous Gaussian chains, commonly known as the Edwards Hamiltonian, and $U_1$ represents the pairwise interaction potential among polymer segments. We assume that the pair potential $u(r)$ between polymer segments separated by a distance of $r$ is of the form $u(r)=k_B T u_0 \delta^3(\mathbf{r})$, where $u_0>0$ characterizes repulsive interactions between polymer segments in a good solvent.[41] For convenience, we adopt the grand canonical description, which is achieved via the standard transformation

$$\mathcal{Z}_G = \sum_{\{n_{l,k}\}=0}^{\infty} e^{\beta \mu_{l,k} n_{l,k}} \mathcal{Z}_C(\{n_{l,k}\}), \tag{A2}$$

where $\mu_{l,k}$ is the chemical potential of the $l$-mer in its $k$th isomeric form. Equations (1) and (2) are recovered from the above by means of a Hubbard–Stratonovich transformation,[41] and by introducing the activities defined as follows:

$$z_{l,k} = \frac{e^{\beta \mu_{l,k}} e^{1/2 f N \beta u(0) l} Z_{0l,k}}{\lambda_T^{3Nfl} V}, \tag{A3}$$

where $u(0)$ denotes the interaction potential at contact, $\lambda_T$ is the de Broglie wavelength of each segment, and $Z_{0l,k}$ denotes the configurational partition function of a noninteracting chain of $l$-mer in its $k$th isomeric form. We emphasize that the combinatorial entropy is contained entirely within the chemical potentials $\mu_{l,k}$ and, hence, the activities $z_{l,k}$, and no information regarding the distribution $\{n_{l,k}\}$ has been employed in obtaining Eqs. (1) and (2).

Information regarding the composition of the equilibrium mixture is contained in Eqs. (3)–(5) via the symmetry numbers $|G_M|$ and $|G_{l,k}|$ appearing in Eq. (5). For a polymer in the graphlike state, the symmetry number is equivalent to the order of the symmetry group (automorphism group[44,45]) of the corresponding unlabeled graph.[13,15] It was established by Gordon and co-workers that the symmetry number $|G_{l,k}|$ and the number of distinct node-rooted, ordered trees that may be formed from the graph of the corresponding isomer $T_{l,k}$ are connected by the relation[13]

$$T_{l,k} = \frac{[(f-1)!]^l (lf)}{|G_{l,k}|}. \tag{A4}$$

This may be seen as follows. A node-rooted tree may be formed from the graph of the $l$-mer by picking a root node in 1 of $l$ possible ways. Subsequently, ordered trees are enumerated by permuting the edges incident on the root node in $f!$ possible ways, corresponding to the $f$ edges emanating from the root node, and the edges emanating from each of the $l-1$ remaining nodes may be permuted in $(f-1)!$ ways. However, some of the resulting trees will be identical, owing to the group of symmetry operations that map the graph onto itself. A division by the number of such symmetry operations, $|G_{l,k}|$, is required in order to obtain the number of distinct rooted, ordered trees, yielding Eq. (A4). Finally, the $f$-arm unit may be assumed to be symmetric to all permutations of its arms, yielding $|G_M|=f!$. Substitution of the above results into Eqs. (3)–(5) yields Eq. (6).

Equation (6) is employed to simplify the entropic contribution to the Hamiltonian in Eq. (2) as follows:

$$\sum_{l=1}^{\infty} \sum_{k} z_{l,k} V Q_{l,k}[iw] = zV \sum_{l=1}^{\infty} \frac{\lambda^{l-1}}{l} \sum_{k} T_{l,k} Q_{l,k}[iw]. \tag{A5}$$

The summation over isomer configurations $k$ for each $l$ may be performed by noticing that the $T_{l,k}$ distinct node-rooted, ordered trees corresponding to the $k$th isomer of $l$ units possess the same partition function $Q_{l,k}$, whereby we obtain

$$\sum_{l=1}^{\infty} \sum_{k} z_{l,k} V Q_{l,k}[iw] = zV \sum_{l=1}^{\infty} \frac{\lambda^{l-1}}{l} Q_l^T[iw]. \tag{A6}$$

In the above, we have introduced the partition function $Q_l^T$ for trees, summed over all distinct node-rooted, ordered trees of $l$ nodes. We may further introduce the propagator to the root node at $\mathbf{r}$ summed over all distinct node-rooted, ordered trees of $l$ nodes via the expression

$$Q_l^T[iw] = \frac{1}{V} \int d^3\mathbf{r} q_l^T(\mathbf{r},[iw]). \tag{A7}$$

The propagator $q_l^T(\mathbf{r},[iw])$ provides the statistical weight for the root node of the tree to lie at position $\mathbf{r}$, summed over all distinct node-rooted, ordered trees of $l$ nodes. While the root node may correspond to different nodes in different trees formed from the same isomer, this is of no consequence to us. Finally, it remains to evaluate the expression

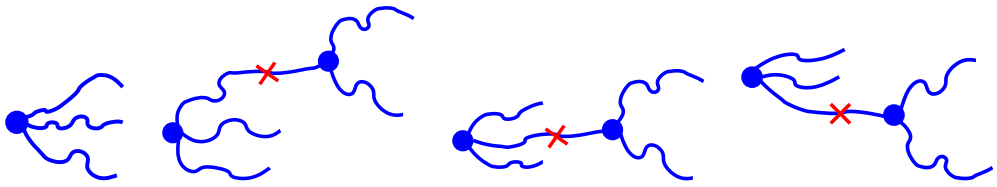

FIG. 11. Distinct rooted, ordered trees having $l=1$ and $l=2$ nodes, with $f=3$. The circles represent nodes and the crosses represent reacted terminals.

$$\sum_{l=1}^{\infty}\sum_{k} z_{l,k} V Q_{l,k}[iw] = z\int d^3\mathbf{r} \sum_{l=1}^{\infty} \frac{\lambda^{l-1}}{l} q_l^{\mathrm{T}}(\mathbf{r},[iw]). \tag{A8}$$

The summation over $l$ is performed by means of generating functions that reproduce all possible tree configurations. We introduce the generating function

$$F_0(\mathbf{r},\theta,[iw]) = \sum_{l=1}^{\infty} \lambda^{l-1} q_l^T(\mathbf{r},[iw])\theta^{l-1} \tag{A9}$$

in the auxiliary variable $\theta$. The coefficient of $\theta^{l-1}$ on the right hand side of Eq. (A9) represents the propagator to the root node at $\mathbf{r}$, summed over all distinct node-rooted, ordered trees of $l$ nodes, incorporating a factor of $\lambda$ for the formation of each of $l-1$ bonds between the $l$ nodes. Therefore, $F_0$ is analogous to a propagator to the root node, summed over all node-rooted, ordered trees of all sizes, with the weighting factors $(\lambda\theta)^{l-1}$ multiplying the contribution from trees of $l$ nodes or $l-1$ bonds. The generating function $F_0$, which constitutes a generating function for the root node at $\mathbf{r}$, may be constructed recursively, yielding Eq. (8). An additional generating function $F_1$, which serves as the generating function for the remaining nodes, has been introduced in Eq. (8). These generating functions reduce to the generating functions defined by Gordon and co-workers[15,18] for homogeneous systems (cf. supplementary material[40]).

Equation (8) implies that $F_0$ possesses the following infinitely nested structure:

$$F_0 = [q_0(N) + \lambda\theta G_{2N} * (q_0(N) + \lambda\theta G_{2N} * (\ldots)^{f-1})^{f-1}]^f, \tag{A10}$$

where we have employed the abbreviated notation $q_0(N) \equiv q_0(\mathbf{r},N,[iw])$, with

$$G_{2N} * f = \int d^3\mathbf{r}' G(\mathbf{r},\mathbf{r}',2N) f(\mathbf{r}') \tag{A11}$$

for any arbitrary function $f(\mathbf{r})$. As defined in Sec. I, $q_0(\mathbf{r},N,[iw])$ denotes the free chain propagator from the free end of an arm to the corresponding node at position $\mathbf{r}$, and the operation $G_{2N}*\ldots$ results in a propagation of the chain conformation by a contour distance of 2 arm lengths from a node to a neighboring bonded node. Therefore, Eqs. (A10) and (8) imply that each of $f$ arms emanating from the root node and $f-1$ arms emanating from the remaining nodes may end in an unreacted terminal or may be bonded to an arm belonging to another node. Consequently, all distinct trees are incorporated in $F_0$. This may be seen by expanding Eq. (A10) into an infinite series, whose terms reproduce all node-rooted, ordered tree configurations with the appropriate weighting factors. For instance, as illustrated by Fig. 11, the term $[q_0(N)]^f$ represents the propagator to the branch point of an unreacted $f$-arm unit, and the term $f[q_0(N)]^{f-1}(\lambda\theta) \times\{G_{2N}*[q_0(N)]^{f-1}\}$ represents dimers, with a weighting factor of $\lambda\theta$ arising from the presence of one bond and the factor of $f$ representing the $f$ distinct ways of ordering the arms incident on the root node.

Finally, Eq. (A9) may be employed to simplify Eq. (A8), yielding

$$\sum_{l=1}^{\infty}\sum_{k} z_{l,k} V Q_{l,k}[iw] = z\int d^3\mathbf{r} \int_0^1 d\theta F_0(\mathbf{r},\theta,[iw]), \tag{A12}$$

which has been utilized in obtaining Eq. (7) from Eq. (2).

The segment density may be obtained from the "factorization property"[41] of the partition function $Q_{l,k}$. From Eq. (11), we obtain

$$\rho(\mathbf{r}) = -zV\sum_{l=1}^{\infty} \frac{\lambda^{l-1}}{l} \frac{\delta Q_l^{\mathrm{T}}[iw]}{\delta iw(\mathbf{r})}. \tag{A13}$$

The above expression is evaluated by computing the contribution from each arm between every node-terminal pair of every distinct node-rooted, ordered tree and summing over all arms in all trees. A tree of $l$ nodes possesses $fl$ arms in all, and therefore, the contribution from a single arm is enhanced by a factor of $fl$. The total segment density is obtained by selecting each of the $l$ nodes of the tree, in turn, as the root node and evaluating the contribution to the segment density from its $f$ arms. Consequently, we obtain the simplified expression for the segment density presented in Eq. (12). The first term in the parentheses on the right hand side of Eq. (12) represents the statistical weight of a segment at a contour distance $s$ measured along the arm from either an unreacted or a reacted terminal, and the second term represents the statistical weight of a segment at a contour distance $N-s$ along the arm measured from the corresponding node. The integral over $\theta$ required in Eq. (A12) is eliminated and a factor of $f$ appears due to the enumeration of $fl$ arms for every tree of $l$ nodes. Upon rewriting Eq. (12) in terms of the scaled variables introduced in Sec. I, we obtain

$$\phi(\bar{\mathbf{r}}) = \bar{z}f\int_0^1 d\bar{s}\Bigg\{\Bigg[q_0(\bar{\mathbf{r}},\bar{s}) + \lambda\theta \times \int d^3\bar{\mathbf{r}}_1 \bar{G}(\bar{\mathbf{r}},\bar{\mathbf{r}}_1,1+\bar{s}) F_1(\bar{\mathbf{r}}_1,\theta)\Bigg] \times \int d^3\bar{\mathbf{r}}_2 \bar{G}(\bar{\mathbf{r}},\bar{\mathbf{r}}_2,1-\bar{s}) F_1(\bar{\mathbf{r}}_2,\theta)\Bigg\}_{\theta=1}, \tag{A14}$$

where we have introduced the scaled Green's function $\bar{G}(\bar{\mathbf{r}},\bar{\mathbf{r}}',\bar{s}) = R^3 G(\mathbf{r},\mathbf{r}',s)$ and the scaled contour variable $\bar{s}$

$=s/N$ for convenience. The field dependence of $q_0$, $\bar{G}$, and $F_1$ is implicit, and it is understood that $q_0$ and $F_1$ are recast in terms of the scaled variables.

The end segment densities[41] may be computed in a similar manner. The total end segment density $\rho_e(\mathbf{r})$ is obtained from Eq. (12) by omitting the integral over $s$ and setting $s=0$ on the right hand side of Eq. (12), yielding

$$\rho_e(\mathbf{r}) = zf\left[1+\lambda\theta\int d^3\mathbf{r}_1 G(\mathbf{r},\mathbf{r}_1,N)F_1(\mathbf{r}_1,\theta,[iw])\right] \times \int d^3\mathbf{r}_2 G(\mathbf{r},\mathbf{r}_2,N)F_1(\mathbf{r}_2,\theta,[iw])|_{\theta=1}. \quad \text{(A15)}$$

The density of unreacted end segments, $\rho_{ue}(\mathbf{r})$, is obtained by retaining only the contribution from unreacted terminals in the first term within the parentheses on the right hand side of Eq. (A15), yielding

$$\rho_{ue}(\mathbf{r}) = zf\int d^3\mathbf{r}' G(\mathbf{r},\mathbf{r}',N)F_1(\mathbf{r}',\theta,[iw])|_{\theta=1}. \quad \text{(A16)}$$

The local fractional density of reacted end segments, $\alpha(\mathbf{r})$, constituting a generalization of Flory's $\alpha$ parameter for an inhomogeneous system, is defined by the expression

$$\alpha(\mathbf{r}) = 1 - \frac{\rho_{ue}(\mathbf{r})}{\rho_e(\mathbf{r})}. \quad \text{(A17)}$$

The segment density of unreacted $f$-arm monomeric units, $\rho_{mon}(\mathbf{r})$, is obtained from the expression

$$\rho_{mon}(\mathbf{r}) = zf\int_0^N ds\left[\int d^3\mathbf{r}' G(\mathbf{r},\mathbf{r}',s)q_0^{f-1}(\mathbf{r}',N)\right]q_0(\mathbf{r},N-s) \quad \text{(A18)}$$

and the corresponding reduced density is obtained as $\phi_{mon}=\rho_{mon}/\rho_0$.

The equilibrium probability $p_l$ for the chain size $l$ in the saddle point approximation is given by $p_l \sim \Sigma_k z_{l,k} V Q_{l,k}$ to within a normalization factor.[41] Consequently, we obtain the number average and weight average degrees of polymerization,

$$N_n = \frac{\Sigma_{l=1}^{\infty}\Sigma_k l z_{l,k} V Q_{l,k}}{\Sigma_{l=1}^{\infty}\Sigma_k z_{l,k} V Q_{l,k}} = \frac{\int_V d^3\mathbf{r} F_0(\mathbf{r},\theta=1)}{\int_0^1 d\theta \int_V d^3\mathbf{r} F_0(\mathbf{r},\theta)} \quad \text{(A19)}$$

and

$$N_w = \frac{\Sigma_{l=1}^{\infty}\Sigma_k l^2 z_{l,k} V Q_{l,k}}{\Sigma_{l=1}^{\infty}\Sigma_k l z_{l,k} V Q_{l,k}} = \frac{\int_V d^3\mathbf{r} \left.\frac{\partial F_0(\mathbf{r},\theta)}{\partial\theta}\right|_{\theta=1}}{\int_V d^3\mathbf{r} F_0(\mathbf{r},\theta=1)} + 1. \quad \text{(A20)}$$

It should be noted that the weight fraction of polymer chains of $l$ units ($\sim\Sigma_k l z_{l,k} V Q_{l,k}$) is proportional to the number of distinct node-rooted, ordered trees of $l$ nodes.[15]

### 2. Pre- and postgelation regimes

The present formulation may equivalently be regarded as a branching process, wherein the root node constitutes the zeroth generation, giving rise successively to the first, second,… generations.[17] Thus, $F_0$ is akin to a probability generating function[20] for the zeroth generation, and $F_1$ for all other generations, since all the remaining nodes are represented by the same generating function $F_1$. The generating function $F_1$ defined by us is, however, normalized such that the partition function $Q_{l,k}[iw]$ reduces to unity in the absence of a field.[41] This normalization differs from the conventional normalization of the probability generating function such that the probabilities of having $0,1,\ldots$ objects in the first generation sum to unity.

The homogeneous system may be represented as a branching process where all the objects are of the same type.[17,20] However, in an inhomogeneous system, the zeroth generation root node at position $\mathbf{r}$ can spawn subsequent generations at any location. Each node is characterized by its spatial location, which is a continuous variable. As an approximation, we model the process as a multitype branching process,[20] where the range of the spatial variable is divided into a finite number of "types." This approximation proves convenient in implementing numerical solutions for inhomogeneous systems, where the domain is invariably discretized. Within this framework, the appropriate statistical weights $F_0$ and $F_1$ may be computed both before the gel point for the sol phase and after the gel point for both sol and gel phases.

Let $Z_{0,j}$ and $Z_{1,j}$ denote the number of objects of type $j$ in the zeroth generation and the first generation, respectively, and let $m_{i,j}$ denote the expected value for the number of objects of type $j$ in the first generation starting from an object of type $i$ in the zeroth generation. Let $\rho$ denote the positive eigenvalue of the matrix of first moments $(m_{i,j})$, which is greater in absolute value than any other eigenvalue. Then, the probability of extinction of the process is unity if $\rho\leq 1$ and is less than unity if $\rho>1$.[20] Furthermore, the probability of extinction must be less than unity starting from objects of all types (in the present case, at all spatial locations) in the latter case.[20] Note that an infinite tree corresponding to the gel phase is formed if the probability of extinction falls below unity. In the homogeneous case, the aforementioned condition leads to the critical value $\alpha_c=1/(f-1)$ for gelation to occur.[17]

In an inhomogeneous system, Eq. (8) yields a nonlinear equation for $F_1$ at the selected discrete spatial locations, which has the form of a vector equation for the vector of values of $F_1$ at the discrete points. Prior to the gel point, the smallest root of $F_1$ at each $\mathbf{r}$ yields the statistical weight for all first generation subtrees rooted at $\mathbf{r}$, which must be finite subtrees. However, beyond the gel point, the smallest root corresponds to the probability of extinction.[17,20] The smallest root of $F_1$ at each $\mathbf{r}$, denoted by $F_1^{fin}$, yields the statistical weight for only the finite first generation subtrees rooted at $\mathbf{r}$, which form the sol phase. The next root of $F_1$ larger than $F_1^{fin}$ at each $\mathbf{r}$, denoted by $F_1^{tot}$, yields the total statistical weight for all first generation subtrees rooted at $\mathbf{r}$, both finite and infinite. Therefore, beyond the gel point, the larger root $F_1^{tot}$ is employed in computing the total density and total conversion. The above procedure is adopted for $\theta\in(0,1]$.

Analogous to Eqs. (12) and (A15)–(A17), expressions for the segment density, end segment densities, and conversion may be defined in the sol phase by employing the sta-

tistical weight for first generation subtrees in the sol phase, $F_1^{\text{fin}}$. These are indicated by the subscript "sol" in Sec. III. The procedure described here constitutes a generalization of Good's method for postgelation calculations in homogeneous systems.[17]


[1] P. Cordier, F. Tournilhac, C. Soulie-Ziakovic, and L. Leibler, Nature (London) **451**, 977 (2008).
[2] J. B. Beck and S. J. Rowan, J. Am. Chem. Soc. **125**, 13922 (2003).
[3] C. Tang, E. M. Lennon, G. H. Fredrickson, E. J. Kramer, and C. J. Hawker, Science **322**, 429 (2008).
[4] T. P. Russell, Science **297**, 964 (2002).
[5] B. Jeong and A. Gutowska, Trends Biotechnol. **20**, 305 (2002).
[6] R. P. Sijbesma, F. H. Beijer, L. Brunsveld, B. J. B. Folmer, J. H. K. K. Hirschberg, R. F. M. Lange, J. K. L. Lowe, and E. W. Meijer, Science **278**, 1601 (1997).
[7] L. Brunsveld, B. J. B. Folmer, E. W. Meijer, and R. P. Sijbesma, Chem. Rev. (Washington, D.C.) **101**, 4071 (2001).
[8] W. J. MacKnight and T. R. Earnest, Jr., J. Polym. Sci. Macromol. Rev. **16**, 41 (1981).
[9] T. Annable, R. Buscall, R. Ettelaie, P. Shepherd, and D. Whittlestone, Langmuir **10**, 1060 (1994).
[10] P. J. Flory, *Principles of Polymer Chemistry* (Cornell University Press, Ithaca, 1953).
[11] W. H. Stockmayer, J. Chem. Phys. **11**, 45 (1943).
[12] M. Gordon and M. Judd, Nature (London) **234**, 96 (1971).
[13] M. Gordon and W. B. Temple, J. Chem. Soc. A, p. 729 (1970).
[14] M. Gordon and G. R. Scantlebury, Trans. Faraday Soc. **60**, 604 (1964).
[15] M. Gordon and W. B. Temple, in *Chemical Applications of Graph Theory*, edited by A. T. Balaban (Academic, London, 1976).
[16] P. G. de Gennes, *Scaling Concepts in Polymer Physics* (Cornell University Press, Ithaca, 1979).
[17] I. J. Good, Proc. R. Soc. London, Ser. A **272**, 54 (1963).
[18] M. Gordon, Proc. R. Soc. London, Ser. A **268**, 240 (1962).
[19] G. R. Dobson and M. Gordon, J. Chem. Phys. **41**, 2389 (1964).
[20] T. E. Harris, *The Theory of Branching Processes* (Springer-Verlag, Berlin, 1963).
[21] I. J. Good, Proc. Cambridge Philos. Soc. **51**, 240 (1955).
[22] I. J. Good, Proc. Cambridge Philos. Soc. **56**, 367 (1960).
[23] M. Gordon and G. N. Malcolm, Proc. R. Soc. London, Ser. A **295**, 29 (1966).
[24] G. R. Dobson and M. Gordon, J. Chem. Phys. **43**, 705 (1965).
[25] M. Ishida and F. Tanaka, Macromolecules **30**, 3900 (1997).
[26] A. N. Semenov and M. Rubinstein, Macromolecules **31**, 1373 (1998).
[27] A. V. Dobrynin, Macromolecules **37**, 3881 (2004).
[28] I. Y. Erukhimovich and A. V. Ermoshkin, J. Exp. Theor. Phys. **88**, 538 (1999).
[29] G. Polya and R. C. Read, *Combinatorial Enumeration of Groups, Graphs and Chemical Compounds* (Springer-Verlag, Berlin, 1987).
[30] Y. Bohbot-Raviv, T. M. Snyder, and Z. G. Wang, Langmuir **20**, 7860 (2004).
[31] P. G. de Gennes, Biopolymers **6**, 715 (1968).
[32] A. Grosberg, A. Gutin, and E. Shakhnovich, Macromolecules **28**, 3718 (1995).
[33] S. Kuchanov, H. Slot, and A. Stroeks, Prog. Polym. Sci. **29**, 563 (2004).
[34] S. Panyukov and Y. Rabin, Phys. Rep. **269**, 1 (1996).
[35] R. C. Ball and S. F. Edwards, Macromolecules **13**, 748 (1980).
[36] S. F. Edwards and T. A. Vilgis, Rep. Prog. Phys. **51**, 243 (1988).
[37] P. Goldbart and N. Goldenfeld, Phys. Rev. Lett. **58**, 2676 (1987).
[38] E. H. Feng, W. B. Lee, and G. H. Fredrickson, Macromolecules **40**, 693 (2007).
[39] R. Elliott and G. H. Fredrickson, J. Chem. Phys. **131**, 144906 (2009).
[40] See supplementary material at http://dx.doi.org/10.1063/1.3497038 for Appendices B–D.
[41] G. H. Fredrickson, *The Equilibrium Theory of Inhomogeneous Polymers* (Oxford University Press, New York, 2006).
[42] D. A. McQuarrie, *Statistical Mechanics* (University Science Books, Sausalito, CA, 2000).
[43] D. A. McQuarrie and J. D. Simon, *Physical Chemistry: A Molecular Approach* (University Science Books, Sausalito, CA, 1997).
[44] K. H. Rosen, J. G. Michaels, J. L. Gross, J. W. Grossman, and D. R. Shier, *Handbook of Discrete and Combinatorial Mathematics* (CRC, Boca Raton, FL, 2000).
[45] F. Harary, *Graph Theory* (Addison-Wesley, Reading, MA, 1969).
[46] R. P. Stanley, *Enumerative Combinatorics* (Cambridge University Press, Cambridge, 1997), Vol. I.
[47] P. Flajolet and R. Sedgewick, *Analytic Combinatorics* (Cambridge University Press, Cambridge, 2009).
[48] M. Frigo and S. G. Johnson, Proc. IEEE **93**, 216 (2005).
[49] W. H. Press, S. A. Teukolsky, W. T. Vetterling, and B. P. Flannery, *Numerical Recipes in C++: The Art of Scientific Computing*, 2nd ed. (Cambridge University Press, New York, 2003).